



# Wiley Analytical Science

## Free Virtual Conference

---

**The 4th edition of the Wiley Analytical Science Conference starts April 26, 2022!**

**Join virtual seminars and connect with key experts during live Q&A sessions.**

**Explore the state of the art methods and advances in:**

- Microscopy
- Lab Automation & Equipment
- Pharma
- Spectroscopy
- Forensics
- Food Science

**[Events.bizzabo.com/WASconferenceSpring22](https://Events.bizzabo.com/WASconferenceSpring22)**

**WILEY**

# In Situ Inorganic Ligand Replenishment Enables Bandgap Stability in Mixed-Halide Perovskite Quantum Dot Solids

Ya-Kun Wang, Kamalpreet Singh, Jiao-Yang Li, Yitong Dong, Xue-Qi Wang, Joao M. Pina, You-Jun Yu, Randy Sabatini, Yang Liu, Dongxin Ma, Jun Liu, Zeke Liu, Yiyuan Gao, Oleksandr Voznyy,\* Wanli Ma, Man-Keung Fung, Liang-Sheng Liao,\* and Edward H. Sargent\*

**Instability in mixed-halide perovskites (MHPs) is a key issue limiting perovskite solar cells and light-emitting diodes (LEDs). One form of instability arises during the processing of MHP quantum dots using an antisolvent to precipitate and purify the dots forming surface traps that lead to decreased luminescence, compromised colloidal stability, and emission broadening. Here, the introduction of inorganic ligands in the antisolvents used in dot purification is reported in order to overcome this problem. MHPs that are colloidally stable for over 1 year at 25 °C and 40% humidity are demonstrated and films that are stable under 100 W cm<sup>-2</sup> photoirradiation, 4× longer than the best previously reported MHPs, are reported. In LEDs, the materials enable an EQE of 24.4% (average 22.5 ± 1.3%) and narrow emission (full-width at half maximum of 30 nm). Sixfold-enhanced operating stability relative to the most stable prior red perovskite LEDs having external quantum efficiency >20% is reported.**

unit solution processing with desirable optoelectronic properties such as tunable light emission and long carrier lifetimes and diffusion lengths.<sup>[9–11]</sup> The rapid development of mixed-halide CsPbBr<sub>x</sub>/I<sub>3–x</sub> nanocrystals via compositional tuning has enabled an EQE of 20.3% in the red with a full-width at half maximum (FWHM) of 40 nm.<sup>[12]</sup> Unfortunately, they have yet to rise to match the operating stability of organic<sup>[13,14]</sup> and inorganic quantum dot<sup>[15,16]</sup> LEDs: device operating stability ( $T_{50}$ ) to date, at an initial luminance of 140 cd m<sup>-2</sup>, has been limited to hours.<sup>[12]</sup>

The organic ligands used in synthesis, and the subsequent exchange, provide colloidal stability in solution. However, these surface ligands are labile, exhibit limited surface binding affinity, and provide high

surface coverage only when present in excess in solution.<sup>[18,19]</sup> They are readily desorbed upon dilution and washing, inducing incomplete passivation of surface sites.

Introducing inorganic ligands in order to better passivate surfaces has shown promising progress in single halide composition in our previous work in both blue and red LEDs.<sup>[10,27]</sup> However, these strategies rely on a highly polar solvent (DMF) to carry out the inorganic salts. The introduction of the highly polar solvent compromises perovskite nanocrystal structural stability and harms the operating stability of LEDs.

Here, we report a strategy wherein we introduce inorganic ligands in the antisolvent used in nanocrystal purification. We show that working with a mildly polar antisolvent, such as ethyl acetate used in this work, allows a gentler processing of the vulnerable perovskite quantum dots. Only by introducing ultrasonication during the introduction of the antisolvent were we able to develop an exchange that was successful, and substantially complete. The inorganic ligands replace, in situ, the organic ligands that are detached from the dot surface (**Figure 1a**): the small inorganic cations provide a rich surface coverage superior to that offered by long-chain organic ligands, and thus prevent trap formation. The inorganic ligands fill surface defects and improve material conductivity and charge-carrier injection in LEDs. The strategy improves bandgap stability, resulting in MHP solids with a storage stability of 1 year in ambient conditions (25 °C and 40% humidity), in comparison to controls that show phase changes after 7 days under the same conditions.

## 1. Introduction


Lead halide perovskites show promise for solar cells,<sup>[1,2]</sup> lasers,<sup>[3,4]</sup> photodetectors,<sup>[5,6]</sup> and light-emitting diodes.<sup>[7,8]</sup> They

Y.-K. Wang, Y. Dong, J. M. Pina, R. Sabatini, D. Ma, E. H. Sargent  
Department of Electrical and Computer Engineering  
University of Toronto  
10 King's College Road, Toronto, Ontario M5S 3G4, Canada  
E-mail: ted.sargent@utoronto.ca

Y.-K. Wang, J.-Y. Li, X.-Q. Wang, Y.-J. Yu, Y. Liu, J. Liu, Z. Liu, Y. Gao,  
W. Ma, M.-K. Fung, L.-S. Liao  
Institute of Functional Nano & Soft Materials (FUNSOM)  
Jiangsu Key Laboratory for Carbon-Based Functional Materials & Devices  
Soochow University  
Suzhou, Jiangsu 215123, P. R. China  
E-mail: lsiao@suda.edu.cn

K. Singh, O. Voznyy  
Department of Physical and Environmental Sciences  
University of Toronto Scarborough  
1065 Military Trail, Scarborough, Ontario M1C 1A4, Canada  
E-mail: o.voznny@utoronto.ca

Y. Dong  
Department of Chemistry and Biochemistry  
University of Oklahoma  
Norman, OK 73019, USA

 The ORCID identification number(s) for the author(s) of this article can be found under <https://doi.org/10.1002/adma.202200854>.

DOI: 10.1002/adma.202200854

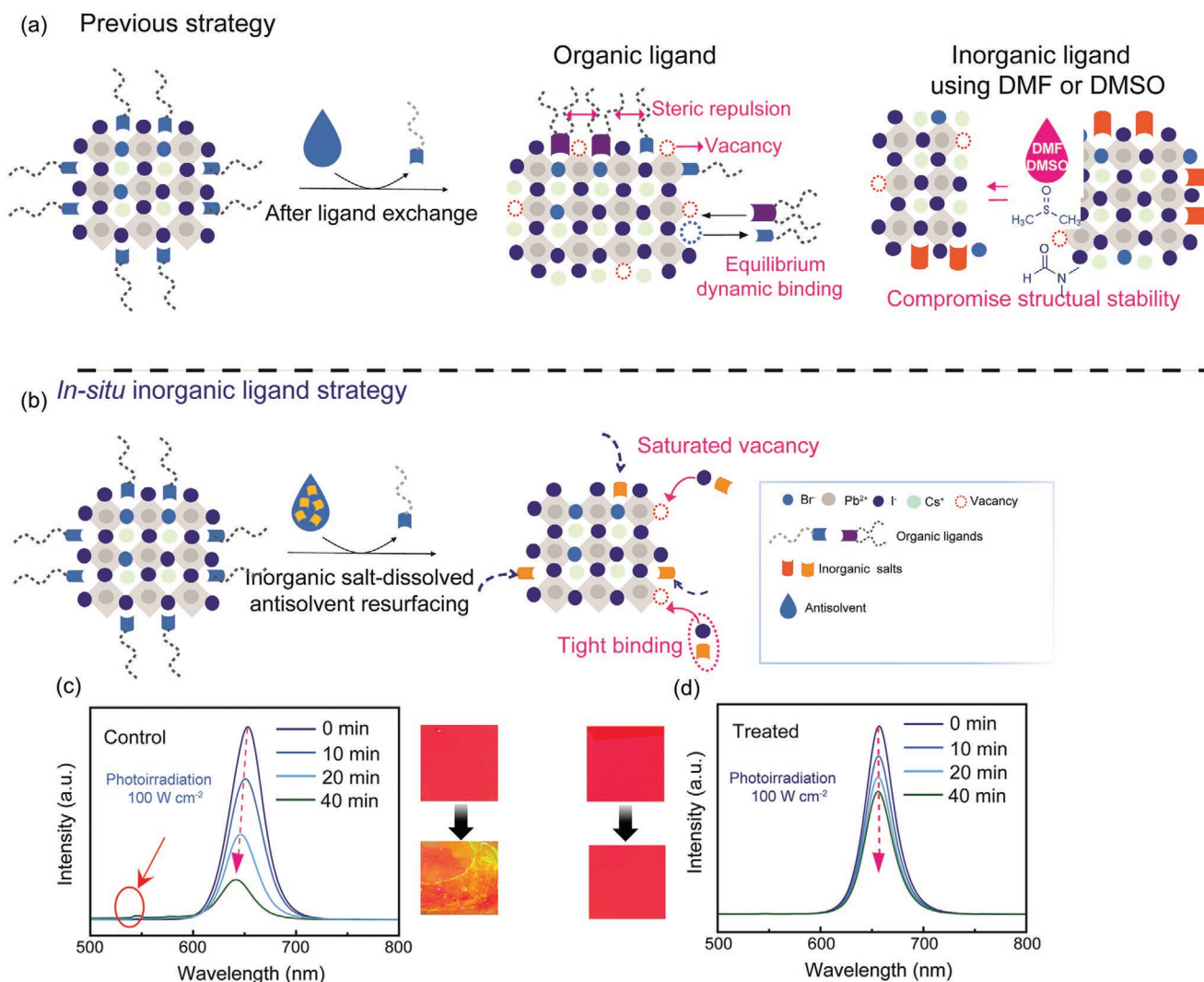


**Figure 1.** In situ inorganic ligand introduction leading to stability under photoirradiation. a) Organic ligands and inorganic ligands were introduced using highly polar solvents. b) The process and advantage of the in situ inorganic ligand strategy via a mildly polar antisolvent. c,d) Bandgap stability of control (c) and treated MHP films (d) under  $100 \text{ W cm}^{-2}$  photoirradiation. The photographs between (c) and (d) show the color change in degraded films after one week.

## 2. Results and Discussion

We began by synthesizing  $\text{CsPb}(\text{I}_x\text{Br}_{1-x})_3$  nanocrystals using a modified ligand-assisted anion-exchange method.<sup>[21]</sup> We then used potassium iodide as the inorganic additive and applied the in situ inorganic ligand strategy (Figure 1b). Similar results were obtained with the use of NaI as the inorganic additive (Figure S1, Supporting Information). For the mild polar solvent, we employed ethyl acetate due to its lower polarity than methyl acetate, making for a more perovskite-friendly solvent. In addition, the ethyl acetate has the appropriate polarity to precipitate the nanocrystals and form a saturated inorganic ligand solution to provide full passivation.

We then investigated the bandgap stability of MHP films. Control  $\text{CsPb}(\text{I}_x\text{Br}_{1-x})_3$  films exhibited a blue-shift in emission after 10 min, ultimately reaching 642 nm, accompanied by broadening of the full-width at half maximum (FWHM). Under

continuous photoirradiation ( $\approx 100 \text{ W cm}^{-2}$ ), a second, higher-energy, photoluminescence peak emerged at 550 nm (Figure 1c), indicating phase segregation of the mixed Br/I perovskites yielding bromine-rich and iodine-rich domains; inefficient energy transfer from the bromine-rich domain to the iodine-rich domain results in an extra peak at  $\approx 550 \text{ nm}$ .<sup>[24,25]</sup> On the other hand, the in situ strategy led to a consistent PL emission profile (Figure 1d) and retention of luminescence intensity, without the emergence of additional peaks and emission broadening. The treated nanocrystal solids are stable under storage for over 1 year at  $25 \text{ }^\circ\text{C}$  and 40% humidity, while controls show phase segregation after 7 days under the same conditions (Figure S2, Supporting Information).

We used time-correlated single-photon counting to investigate the surface trap density of the  $\text{CsPb}(\text{I}_x\text{Br}_{1-x})_3$  nanocrystals. The treated films showed a longer radiative lifetime compared to controls (50 vs 30 ns, Figure 2a) along with a greater PLQY



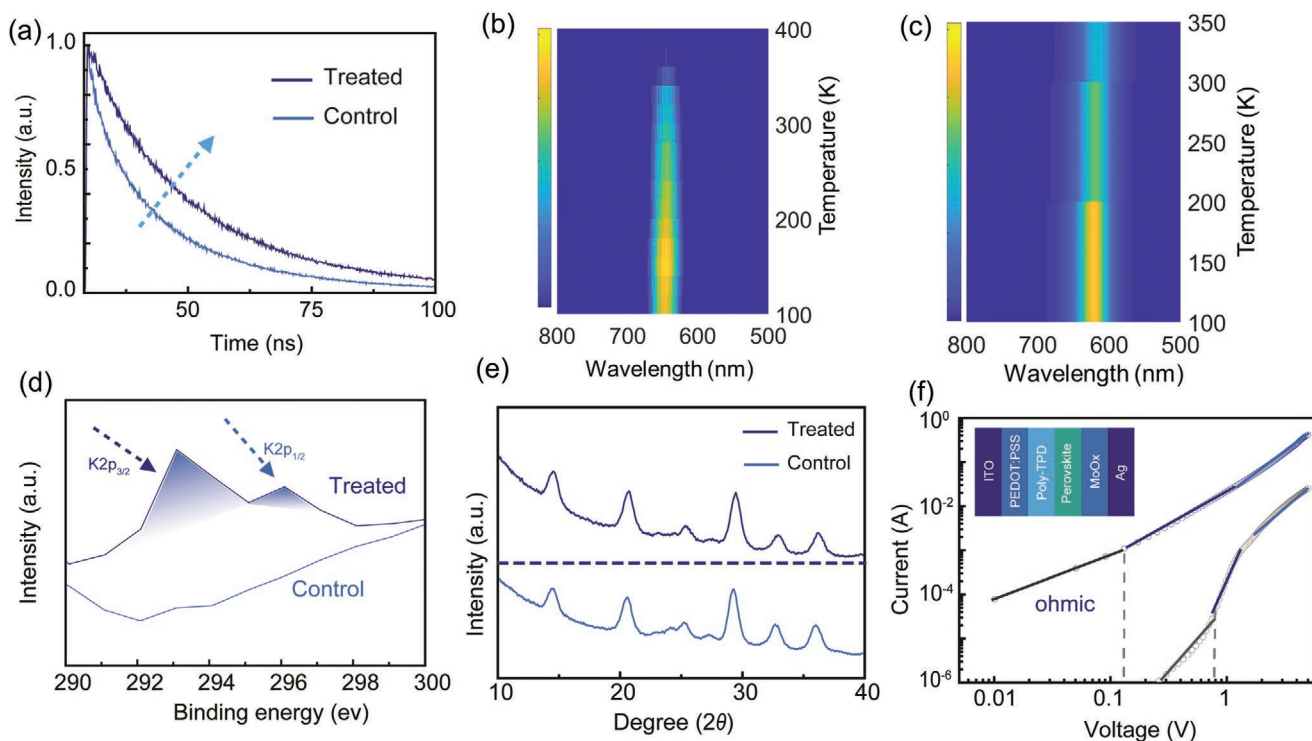


**Figure 2.** Photoluminescence lifetime, carrier mobility, and bandgap stability in films compared to controls. a) Time-resolved photoluminescence (TRPL) decay of control and treated films. b,c) Bandgap stability of in situ inorganic ligand treated  $\text{CsPb}(\text{I}_x\text{Br}_{1-x})_3$  (b) and control (c) films at different temperatures. d) XPS spectra of  $\text{CsPb}(\text{I}_x\text{Br}_{1-x})_3$  nanocrystal films in the K2p detection range. e) XRD of control and treated films. f) Current density–voltage curves of a representative hole-only device under dark conditions. The inset shows the device structure.

(95% for treated films vs to 62% for controls). These results suggest that the in situ inorganic ligand is useful in improving the photophysical properties of the MHP nanocrystals. When exposed to temperatures of 100 °C for 30 min, the treated samples show stable emission (Figure 2b and Figure S3a, Supporting Information), in contrast to controls (Figure 2c and Figure S3b, Supporting Information).

Next, we used XPS and XRD to characterize the composition and structure of MHP films. XPS of the treated films exhibits a K2p peak in the range of 290–300 eV, while the additive-free control films lack features in this range (Figure 2d). XRD measurements (Figure 2e) indicate a cubic phase with a lattice constant of 6.10 Å for nanocrystal films with and without treatment. The incorporation of the inorganic ligand is supported by a redshift in emission (Figure S4a, Supporting Information) and the presence of a K2p peak in the XPS of treated samples. The HRTEM of the treated sample maintains a more homogenous size distribution than the controls due to the well-passivation surface endowed by in situ inorganic ligand treatment (Figure S4b, Supporting Information). Space-charge-limited-current (SCLC) measurements (Figure 2f) show that the charge mobility of nanocrystal films after treatment increases from  $9 \times 10^{-4} \text{ cm}^2 \text{ V}^{-1} \text{ s}^{-1}$  to  $6 \times 10^{-2} \text{ cm}^2 \text{ V}^{-1} \text{ s}^{-1}$ .<sup>[26,27]</sup>

We studied, as controls, the use of pure antisolvent (Figure 3a) and also investigated the use of high-solubility organic ligands alone (Figure 3b). A shoulder at higher energy emerged in each case following continuous irradiation,<sup>[28,29]</sup> while in situ inorganic ligand treated samples maintained a consistent emission

profile (Figure 3c). The failure to generate stable films using organic ligands is attributed to ligand loss upon antisolvent wash, which leads to vacancies that facilitate phase segregation.

To investigate the ligand loss phenomenon, density functional theory (DFT) simulations were employed to probe the impact of surface ligand coverage on the formation of surface halide vacancies. Our calculations showed that the energy needed to remove an iodide from a partially covered surface is  $\approx 0.25$  eV lower compared to the fully covered counterpart (Figure S5, Supporting Information). This finding supports the notion that increased surface coverage from inorganic cations in the antisolvent suppresses the generation of halide vacancies and related phase segregation.

To further explore the ability of the in situ inorganic ligand strategy in protecting the surface, we investigated the anion exchange process with and without treatment. In transient absorption, additive-free controls showed two bleach peaks, one at 480 nm and the other at 540 nm, which we assign to  $\text{CsPbBr}_3$  and  $\text{CsPb}(\text{I}_x\text{Br}_{1-x})_3$ , respectively<sup>[30]</sup> (Figure 3d). The organic ligand treated samples showed reduced halide vacancies compared to antisolvent-only samples, but the shift of bleach peaks to below 600 nm (Figure 3e) indicates incomplete stability. By contrast, the in situ inorganic additive treated samples show a bleach peak fixed in its original position (Figure 3f).

We sought to assess the nanocrystals in light-emitting diodes (LEDs). A schematic of the device stack with the energy level of each layer is shown in Figure 4a. The energy levels of

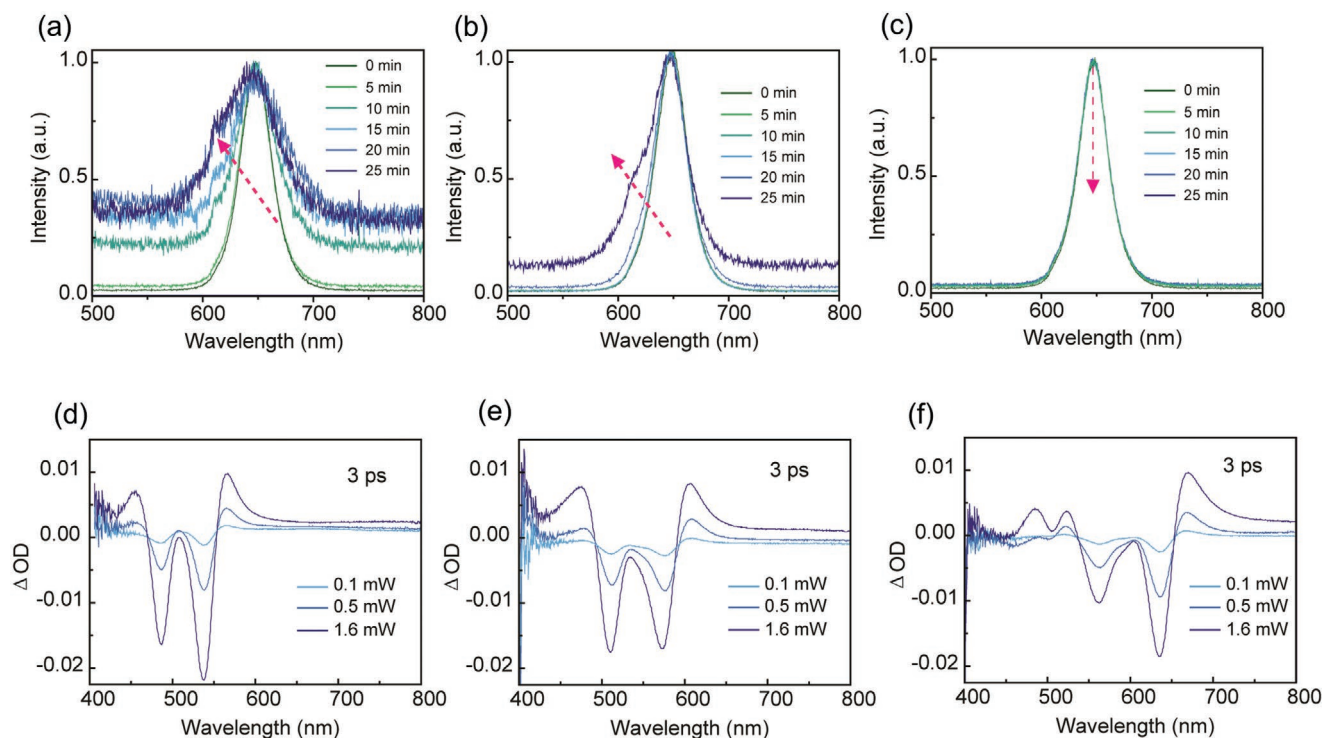


**Figure 3.** In situ PL and femtosecond transient absorption. a–c) PL spectra of  $\text{CsPb}(\text{I}_x\text{Br}_{1-x})_3$  samples treated with antisolvent alone (a); and with oleylamine iodide (b); all as a function of time under  $100 \text{ W cm}^{-2}$  photoirradiation; this is compared with in situ inorganic ligand treated samples (c) under the same conditions of irradiation. d–f) Transient absorption spectra of control  $\text{CsPb}(\text{I}_x\text{Br}_{1-x})_3$  samples treated with antisolvent alone (d); and with oleylamine iodide (e) versus in situ inorganic ligand treated samples (f) with three different powers recorded at a time delay of 3 ps.

perovskites were calculated from optical data and ultraviolet photoelectron spectroscopy (Figure S6, Supporting Information). The LED employed an ITO glass substrate anode, poly(3,4-ethylenedioxythiophene):poly(styrene-sulfonate) mixed with PFI as a hole-injection layer (HIL), a poly(bis-4butylphenyl-*N,N*-bisphenyl)benzidine) hole-transport layer (HTL), an active  $\text{CsPb}(\text{I}_x\text{Br}_{1-x})_3$  emission layer, a 3',3''',3''''-(1,3,5-triazine-2,4,6-triyl)tris([1,1'-biphenyl]-3-carbonitrile) electron-transport layer (ETL), and a LiF/Al double-layered cathode.

In situ inorganic ligand treated LEDs required a lower driving voltage ( $2.6 \text{ V}$  at  $100 \text{ cd m}^{-2}$ ) than did controls ( $\approx 3.3 \text{ V}$  at  $100 \text{ cd m}^{-2}$ ) (Figures 4b–d). This drive voltage is among the lowest for  $\text{CsPb}(\text{I}_x\text{Br}_{1-x})_3$  based perovskite red LEDs.<sup>[12,21,27]</sup> Champion devices exhibited an external quantum efficiency for red perovskite LEDs (Figures 4c,d): the highest  $\text{EQE}_{\text{max}}$  herein, 24.4%, is 1.1-fold greater than in the highest-EQE  $\text{CsPbBr}_x/\text{I}_{3-x}$  red perovskite LED prior report.<sup>[21]</sup> Additionally, the luminance at maximum EQE is 1.3× higher than that recently demonstrated in  $\text{CsPb}(\text{I}_x\text{Br}_{1-x})_3$ .<sup>[12]</sup> Compared to control devices (Figure 4e), we observed a 1.4× narrower EL profile (30 and 42 nm) in the treated LEDs. The control LEDs exhibited a progressive broadening of the emission peak when the current density was increased from 1 to  $10 \text{ mA cm}^{-2}$ . At  $20 \text{ mA cm}^{-2}$ , the broadening intensified, and this was accompanied by a 2 nm redshift (Figure 4f). By contrast, the emission profile for the treated LEDs is stable under the same progressively increasing drive conditions (Figure 4g). Figure 4h shows the EQE histogram of 15 devices. Angle-dependent

electroluminescence (EL) measurements (Figure 4i) reveal that the radiation patterns are Lambertian.<sup>[31]</sup> The better morphology of treated films also contributes to better device performance (Figure S7, Supporting Information).

We then monitored the surface temperature variation at even driving electrical currents ( $150 \text{ mA cm}^{-2}$ ) to challenge further the bandgap stability of the treated LEDs. The emission was stable even as Joule heating increased the steady-state temperature to  $\approx 40 \text{ }^\circ\text{C}$  (Figure S8, Supporting Information). We investigated the LED operating lifetime, monitoring the luminescence as a function of time: at an initial luminance of  $290 \text{ cd m}^{-2}$ , the  $T_{50}$  (time to decay to 50% of its initial value) was  $\approx 20 \text{ h}$  (Figure 4j), a sixfold increase relative to the most stable prior red perovskite LEDs having EQEs exceeding 20% (Table S1, Supporting Information).<sup>[12,21,27]</sup>

### 3. Conclusion

This work reports an antisolvent-assisted in situ inorganic ligand strategy that increases the bandgap stability of MHPs. Introducing the inorganic ligand in the antisolvent helps to saturate surface traps caused by the removal of organic ligands during nanocrystal purification, and in improving c-NC conductivity for LEDs. The strategy leads to MHP nanocrystals with a colloidal stability of 1 year under ambient conditions; and thin films stable under photoirradiation and electrical bias. LEDs exhibited an EQE of 24.4% and the longest

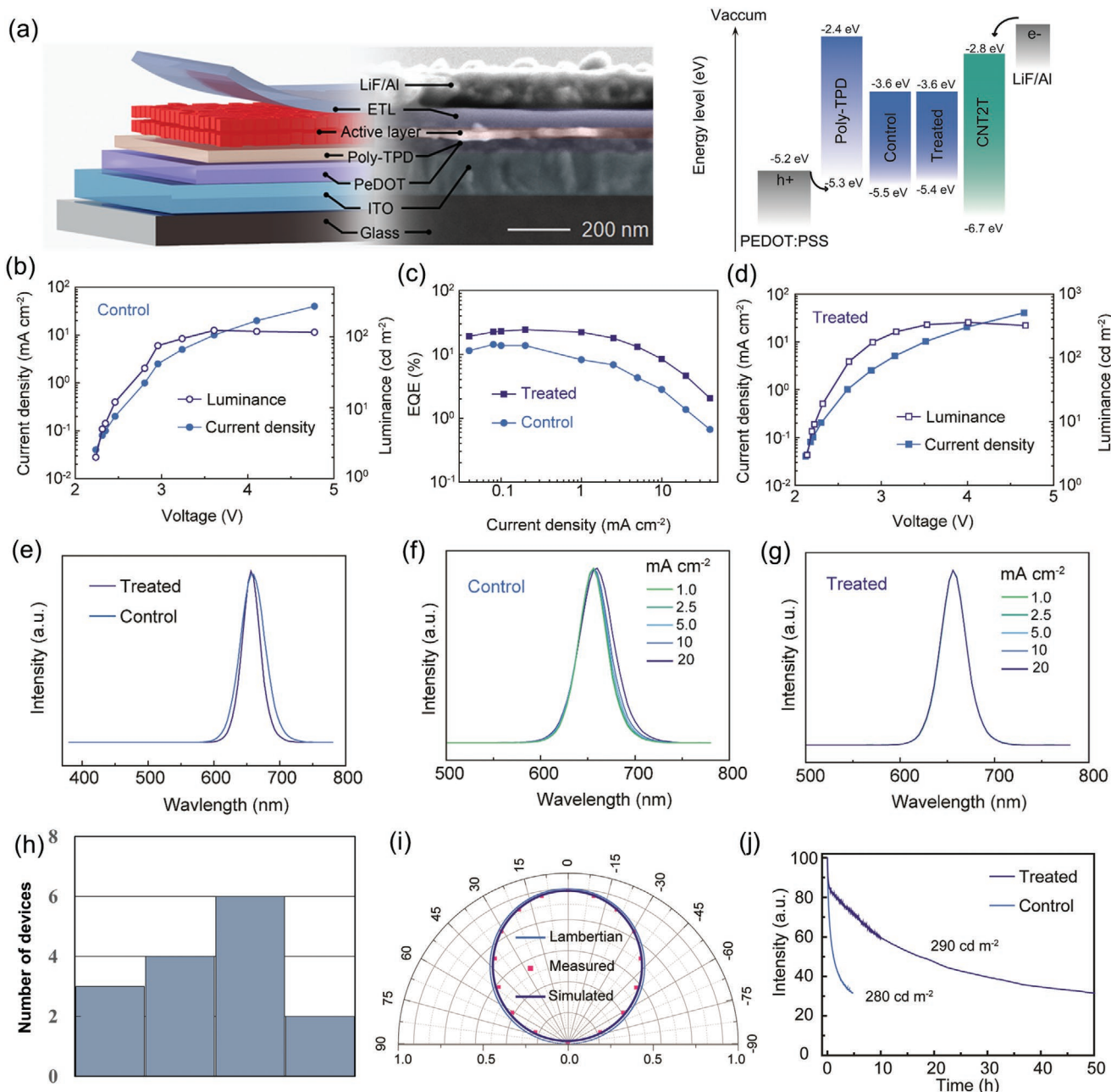


**Figure 4.** LED performance. a) Device structure, cross-sectional SEM image, and energy band diagram. The energy levels of the CsPb(I<sub>x</sub>Br<sub>1-x</sub>)<sub>3</sub> were calculated from ultraviolet photoelectron spectroscopy (UPS in Figure S6, Supporting Information). b) Current density–voltage–luminance curves of control LEDs. c) EQE versus current density curve of treated LEDs. d) Current density–voltage–luminance curves of treated LEDs. e) EL spectra of control and treated LEDs. f,g) EL stability under different current densities of control (f) and treated (g) LEDs. h) EQE histogram of 15 devices. i) Lambertian profile of treated LEDs. j) Operating stability at a luminance of 290 and 280 cd m<sup>-2</sup> for treated and control LEDs, respectively.

operating stability among red perovskite LEDs having EQE over 20%.

## Supporting Information

Supporting Information is available from the Wiley Online Library or from the author.

## Acknowledgements

The authors acknowledge financial support from the Natural Science Foundation of China (Nos. 51821002, 91733301). This work was supported by the Natural Sciences and Engineering Research Council of Canada (NSERC grant numbers 216956-12 and 2019-04897), China Postdoctoral Science Foundation (2021M690114 and 2021TQ0230), and the Collaborative Innovation Center of Suzhou Nano Science and Technology. Computations were performed on the Niagara

supercomputer at the SciNet HPC Consortium. SciNet was funded by the Canada Foundation for Innovation; the Government of Ontario; and the University of Toronto.

## Conflict of Interest

The authors declare no conflict of interest.

## Data Availability Statement

The data that support the findings of this study are available from the corresponding author upon reasonable request.

## Keywords

bandgap stability, in situ ligand exchange, mixed-halide perovskites, operational stability, perovskite LEDs

Received: January 26, 2022

Revised: March 7, 2022

Published online:

- [1] M. A. Green, A. Ho-Baillie, H. J. Snaith, *Nat. Photonics* **2014**, *8*, 506.
- [2] National Renewable Energy Laboratory, Best Research-Cell Efficiency Chart, <https://www.nrel.gov/pv/cell-efficiency.html> (accessed: March 2021).
- [3] F. Deschler, M. Price, S. Pathak, L. E. Klintberg, D.-D. Jarausch, R. Higler, S. Hüttner, T. Leijtens, S. D. Stranks, H. J. Snaith, M. Atatüre, R. T. Phillips, R. H. Friend, *J. Phys. Chem. Lett.* **2014**, *5*, 1421.
- [4] G. Xing, N. Mathews, S. S. Lim, N. Yantara, X. Liu, D. Sabba, M. Grätzel, S. Mhaisalkar, T. C. Sum, *Nat. Mater.* **2014**, *13*, 476.
- [5] Y. Fang, Q. Dong, Y. Shao, Y. Yuan, J. Huang, *Nat. Photonics* **2015**, *9*, 679.
- [6] C. Li, H. Wang, F. Wang, T. Li, M. Xu, H. Wang, Z. Wang, X. Zhan, W. Hu, L. Shen, *Light Sci. Appl.* **2020**, *9*, 31.
- [7] L. N. Quan, B. P. Rand, R. H. Friend, S. G. Mhaisalkar, T.-W. Lee, E. H. Sargent, *Chem. Rev.* **2019**, *119*, 7444.
- [8] Z.-K. Tan, R. S. Mghaddam, M. L. Lai, P. Docampo, R. Higler, F. Deschler, M. Price, A. Sadhanala, L. M. Pazos, D. Credgington, F. Hanusch, T. Bein, H. J. Snaith, R. H. Friend, *Nat. Nanotechnol.* **2014**, *9*, 687.
- [9] X. Yang, X. Zhang, J. Deng, Z. Chu, Q. Jiang, J. Meng, P. Wang, L. Zhang, Z. Yin, J. You, *Nat. Commun.* **2018**, *9*, 570.
- [10] Y. Dong, Y.-K. Wang, F. Yuan, A. Johnston, Y. Liu, D. Ma, M.-J. Choi, B. Chen, M. Chekini, S.-W. Baek, L. K. Sagar, J. Fan, Y. Hou, M. Wu, S. Lee, B. Sun, S. Hoogland, R. Quintero-Bermudez, H. Ebe, P. Todorovic, F. Dinic, P. Li, H. T. Kung, M. I. Saidaminov, E. Kumacheva, E. Spiecker, L.-S. Liao, O. Voznyy, Z.-H. Lu, E. H. Sargent, *Nat. Nanotechnol.* **2020**, *15*, 668.
- [11] D. Shi, V. Adinolfi, R. Comin, M. Yuan, E. Alarousu, A. Buin, Y. Chen, S. Hoogland, A. Rothenberger, K. Katsiev, Y. Losovyj, X. Zhang, P. A. Dowben, O. F. Mohammed, E. H. Sargent, O. M. Bakr, *Science* **2015**, *347*, 519.
- [12] Y. Hassan, J. H. Park, M. L. Crawford, A. Sadhanala, J. Lee, J. C. Sadighian, E. Mosconi, R. Shivanna, E. Radicchi, M. Jeong, C. Yang, H. Choi, S. H. Park, M. H. Song, F. De Angelis, C. Y. Wong, R. H. Friend, B. R. Lee, H. J. Snaith, *Nature* **2021**, *591*, 72.
- [13] S. Hirata, Y. Sakai, K. Masui, H. Tanaka, S. Y. Lee, H. Nomura, N. Nakamura, M. Yasumatsu, H. Nakanotani, Q. Zhang, K. Shizu, H. Miyazaki, C. Adachi, *Nat. Mater.* **2015**, *14*, 330.
- [14] X. Tang, L.-S. Cui, H.-C. Li, A. J. Gillett, F. Auras, Y.-K. Qu, C. Zhong, S. T. E. Jones, Z.-Q. Jiang, R. H. Friend, L.-S. Liao, *Nat. Mater.* **2020**.
- [15] Y.-H. Won, O. Cho, T. Kim, D.-Y. Chung, T. Kim, H. Chung, H. Jang, J. Lee, D. Kim, E. Jang, *Nature* **2019**, *575*, 634.
- [16] T. Kim, K.-H. Kim, S. Kim, S.-M. Choi, H. Jang, H.-K. Seo, H. Lee, D.-Y. Chung, E. Jang, *Nature* **2020**, *586*, 385.
- [17] J. De Roo, M. Ibáñez, P. Geiregat, G. Nedelcu, W. Walravens, J. Maes, J. C. Martins, I. Van Driessche, M. V. Kovalenko, Z. Hens, *ACS Nano* **2016**, *10*, 2071.
- [18] Y. Bai, M. Hao, S. Ding, P. Chen, L. Wang, *Adv. Mater.* **2021**, *34*, 2105958.
- [19] Y. Dong, T. Qiao, D. Kim, D. Parobek, D. Rossi, D. H. Son, *Nano Lett.* **2018**, *18*, 3716.
- [20] G. Almeida, I. Infante, L. Manna, *Science* **2019**, *364*, 833.
- [21] T. Chiba, Y. Hayashi, H. Ebe, K. Hoshi, J. Sato, S. Sato, Y.-J. Pu, S. Ohisa, J. Kido, *Nat. Photonics* **2018**, *12*, 681.
- [22] M. Abdi-Jalebi, Z. Andaji-Garmaroudi, S. Cacovich, C. Stavrakas, B. Philippe, J. M. Richter, M. Alsari, E. P. Booker, E. M. Hutter, A. J. Pearson, S. Lilliu, T. J. Savenije, H. Rensmo, G. Divitini, C. Ducati, R. H. Friend, S. D. Stranks, *Nature* **2018**, *555*, 497.
- [23] M. Abdi-Jalebi, Z. Andaji-Garmaroudi, A. J. Pearson, G. Divitini, S. Cacovich, B. Philippe, H. Rensmo, C. Ducati, R. H. Friend, S. D. Stranks, *ACS Energy Lett.* **2018**, *3*, 2671.
- [24] Q. Jiang, Y. Zhao, X. Zhang, X. Yang, Y. Chen, Z. Chu, Q. Ye, X. Li, Z. Yin, J. You, *Nat. Photonics* **2019**.
- [25] B. Murali, E. Yengel, C. Yang, W. Peng, E. Alarousu, O. M. Bakr, O. F. Mohammed, *ACS Energy Lett.* **2017**, *2*, 846.
- [26] H. Xu, X. Wang, Y. Li, L. Cai, Y. Tan, G. Zhang, Y. Wang, R. Li, D. Liang, T. Song, B. Sun, *J. Phys. Chem. Lett.* **2020**, *11*, 3689.
- [27] Y.-K. Wang, F. Yuan, Y. Dong, J.-Y. Li, A. Johnston, B. Chen, M. I. Saidaminov, C. Zhou, X. Zheng, Y. Hou, K. Bertens, H. Ebe, D. Ma, Z. Deng, S. Yuan, R. Chen, L. K. Sagar, J. Liu, J. Fan, P. Li, X. Li, Y. Gao, M.-K. Fung, Z.-H. Lu, O. M. Bakr, L.-S. Liao, E. H. Sargent, *Angew. Chem., Int. Ed.* **2021**, *60*, 16164.
- [28] Y. Zhou, Y.-H. Jia, H.-H. Fang, M. A. Loi, F.-Y. Xie, L. Gong, M.-C. Qin, X.-H. Lu, C.-P. Wong, N. Zhao, *Adv. Funct. Mater.* **2018**, *28*, 1803130.
- [29] H. Zhang, X. Fu, Y. Tang, H. Wang, C. Zhang, W. W. Yu, X. Wang, Y. Zhang, M. Xiao, *Nat. Commun.* **2019**, *10*, 1088.
- [30] C. G. Bischak, C. L. Hetherington, H. Wu, S. Aloni, D. F. Ogletree, D. T. Limmer, N. S. Ginsberg, *Nano Lett.* **2017**, *17*, 1028.
- [31] Y.-H. Kim, S. Kim, A. Kakekhani, J. Park, J. Park, Y.-H. Lee, H. Xu, S. Nagane, R. B. Wexler, D.-H. Kim, S. H. Jo, L. Martínez-Sarti, P. Tan, A. Sadhanala, G.-S. Park, Y.-W. Kim, B. Hu, H. J. Bolink, S. Yoo, R. H. Friend, A. M. Rappe, T.-W. Lee, *Nat. Photonics* **2021**, *15*, 148.